Title: Engineered receptor binding domain immunogens elicit pan-coronavirus neutralizing antibodies

Authors: Blake M. Hauser[1*], Maya Sangesland[1*], Evan C. Lam[1], Jared Feldman[1], Ashraf S. Yousif[1], Timothy M. Caradonna[1], Alejandro B. Balazs[1], Daniel Lingwood[1] and Aaron G. Schmidt[1,2]

[1]Ragon Institute of MGH, MIT and Harvard, Cambridge, MA, 02139, USA

[2]Department of Microbiology, Harvard Medical School, Boston, MA 02115, USA

Key words: immunogen design, protein engineering, broadly neutralizing antibodies, SARS-CoV-2, coronavirus

*equal contribution

Correspondence:

Daniel Lingwood
Tel:857-268-7180; E-mail: dlingwood@mgh.harvard.edu

Aaron G. Schmidt
Tel: 857-268-7118; E-mail: aschmidt@crystal.harvard.edu

Running title: Eliciting cross-neutralizing antibodies with a pan-coronavirus vaccine

Abstract

Effective countermeasures are needed against emerging coronaviruses of pandemic potential, similar to severe acute respiratory syndrome coronavirus 2 (SARS-CoV-2). Designing immunogens that elicit broadly neutralizing antibodies to conserved viral epitopes on the major surface glycoprotein, spike, such as the receptor binding domain (RBD) is one potential approach. Here, we report the generation of homotrimeric RBD immunogens from different sarbecoviruses using a stabilized, immune-silent trimerization tag. We find that that a cocktail of homotrimeric sarbecovirus RBDs can elicit a neutralizing response to all components even in context of prior SARS-CoV-2 imprinting. Importantly, the cross-neutralizing antibody responses are focused towards conserved RBD epitopes outside of the ACE-2 receptor-binding motif. This may be an effective strategy for eliciting broadly neutralizing responses leading to a pan-sarbecovirus vaccine.

Main Text

The emergence of the novel severe acute respiratory syndrome coronavirus 2 (SARS-CoV-2) and the subsequent global pandemic has highlighted the disruptive threat posed by viruses for which humans have no prior immunity. Rapid development of potential vaccines has led to an unprecedented 13 candidates already in Phase 3 clinical trials in the last 6 months; while differing in modality (e.g., mRNA, adenovirus), the primary immunogen for many of these candidates is the SARS-CoV-2 spike ectodomain (*1*). With the continued global spread of SARS-CoV-2, in conjunction with potential vaccinations, it is likely that a large proportion of the global population will eventually develop an immune response to SARS-CoV-2. However, even after potentially achieving herd immunity sufficient to slow the spread of SARS-CoV-2, there remains a constant threat of emerging coronaviruses with pandemic potential. Indeed, surveillance efforts have identified numerous unique coronaviruses within various animal reservoirs, raising the possibility of zoonotic transmission (*2, 3*). Such events are likely to increase in frequency as a result of human impact on the environment (*4*). While the current SARS-CoV-2 pandemic has an estimated infection fatality rate of between ~1-2%, with numerous cases likely undetected, previous SARS-CoV and MERS-CoV outbreaks were more lethal with ~10% and ~35% case fatality rates, respectively, raising the possibility that future novel coronaviruses have potentially high mortality (*5-7*). Additionally, elicited immunity to SARS-CoV-2 infection may not protect against even closely related novel coronaviruses from the same sarbecovirus subgenus (*8*). It is therefore critical to not only address the current pandemic, but also develop vaccine platforms that can be readily adapted to potential emerging coronaviruses.

While we cannot readily predict which coronaviruses will next emerge into the human population, a proactive approach to generate broadly protective immunity is to design immunogens that elicit humoral responses targeting conserved sites on the coronavirus spike glycoprotein. Such sites may include the receptor binding domain which engages host-cell receptors necessary to facilitate viral cell entry; these spike-mediated interactions are conserved across coronaviruses (*9*). Indeed, a subset of spike-directed antibodies from convalescent patients can potently neutralize SARS-CoV-2; comparable neutralizing antibodies against SARS-CoV and MERS-CoV have also been identified (*6, 10-15*). Some spike-directed antibodies that neutralize SARS-CoV-2 also bind the SARS-CoV spike protein, highlighting the presence of cross-reactive neutralizing epitopes (*10,*

87 *16, 17*). Multimerized versions of the receptor binding domains (RBDs) of several coronaviruses
88 have previously been shown to be potent immunogens (*18*). Here, we describe a customizable
89 vaccine that elicits pan-sarbecovirus neutralization against both SARS-CoV-2 and the potentially
90 emergent WIV1-CoV (*19*). This approach focuses antibody responses to conserved, protective
91 RBD epitopes shared across sarbecoviruses. Its flexible nature allows facile interchanging of
92 potential vaccine strains updated to confer neutralization against new emerging coronaviruses.
93 Importantly, this approach was applied in context of "pre-existing" SARS-CoV-2 humoral
94 immunity with the goal of broadening neutralization while simultaneously boosting the
95 neutralizing antibody response to SARS-CoV-2, similar to the "back boost" effect of seasonal
96 influenza immunizations (*20*). Thus, it has the potential to provide protection against currently
97 circulating SARS-CoV-2, while proactively generating neutralizing antibody responses against
98 emerging coronaviruses.
99
100 We designed a cystine-stabilized and hyperglycosylated variant of a GCN4 trimerization tag to
101 generate a homotrimeric immunogen "cassette" to rapidly exchange RBDs from various
102 coronaviruses (**Figure 1A, S1**). Using a hyperglycosylated GCN4 allows the RBDs to remain
103 trimerized while the tag is "immune silent" (*21*). As a proof-of-concept for our immunization
104 approach, we selected the SARS-CoV, SARS-CoV-2, and WIV1-CoV RBDs as our starting
105 immunogens. We overexpressed RBD homotrimers in mammalian cells to maximize glycan
106 complexity and purified to homogeneity via size exclusion chromatography; the trimeric species
107 was confirmed using SDS-PAGE analysis under non-reducing conditions (**Figure 1B-C**). Their
108 antigenicity was assayed using conformational-specific antibodies CR3022 and/or B38 using
109 biolayer interferometry; the RBD homotrimers had comparable affinities in comparison to RBD
110 monomers (**Figure S2**). The purification tags were removed by enzymatic cleavage prior to
111 immunization.
112
113 To understand how preexisting immunity to SARS-CoV-2, whether acquired through natural
114 infection or vaccination, could affect immune responses to our immunogens, we primed our
115 cohorts with recombinant spike or RBD protein (*22, 23*). Our two control arms followed this prime
116 with subsequent homologous boosts of recombinant SARS-CoV-2 spike ("spike" cohort) or RBD
117 ("RBD" cohort); the latter is necessary for comparing the effect on immunogencity of monomeric

118 versus trimeric RBDs. Our experimental arms both received the spike prime and included a SARS-
119 CoV-2 RBD homotrimer boost ("homotrimer" cohort) and an equimolar boosting cocktail of
120 SARS-CoV-2, SARS-CoV, and WIV1-CoV RBD homotrimers ("cocktail" cohort) (**Figure 2A**).
121 All cohorts received the same total amount of protein in each immunization. We evaluated the
122 serum response against coronavirus-derived antigens using ELISAs (**Figure 2B-C, S3**). All four
123 immunization regimens resulted in similar patterns of serum reactivity. Each cohort demonstrated
124 a significant decrease in reactivity against SARS-CoV RBD as compared to the SARS-CoV-2
125 RBD or spike, though the magnitude of this difference was relatively small. The cohort which
126 received the RBD homotrimer cocktail boost had the highest overall endpoint titers, while the
127 cohort that received the monomeric SARS-CoV-2 RBD had the lowest overall endpoint titers; the
128 latter observation is consistent with other previous reports and likely due to the inefficiency of
129 monomeric RBDs effectively stimulating B cell receptors. We confirmed the non-immunogenic
130 nature of the hyperglycosylated GCN4 tag by assaying sera from the wildtype homotrimer cocktail
131 boost against another viral glycoprotein, hemagglutinin, with the same tag (**Figure S4**).
132
133 We next evaluated whether the serum response was directed towards cross-reactive, and
134 potentially broadly neutralizing RBD epitopes. Conservation across SARS-CoV-2, SARS-CoV,
135 and WIV1-CoV RBDs primarily occurs outside of the ACE-2 receptor binding motif (RBM)
136 (**Figure S5A**). Indeed, the previously characterized CR3022 and S309 antibodies have footprints
137 that together cover much of this conserved region, with epitope buried surface area (BSA) of 917
138 $Å^2$ and 795 $Å^2$ respectively in comparison to BSA of 869 $Å^2$ for ACE-2 (*16, 17, 24*). We performed
139 serum competition by incubating RBD-coated ELISA plates with IgGs B38, P2B-2F6, CR3022,
140 and S309, representing each of the four previously defined "classes" of SARS-CoV-2 RBD
141 epitopes (*25*) (**Figure S5B**). We then assessed binding of mouse serum IgG. In all cohorts,
142 competition with both CR3022 and S309 significantly reduced serum titers against the SARS-CoV
143 and WIV1-CoV RBDs (**Figure 2D**). However, only the cohort receiving the RBD homotrimer
144 cocktail showed a significant reduction in serum titers against the SARS-CoV-2 RBD in
145 competition with both CR3022 and S309 ($p = 0.0340$) (**Figure 2D**). This result suggests a higher
146 degree of focusing to this region elicited specifically by the homotrimer cocktail immunogens.
147

148 To compare to the observed sera responses, we measured the IgG B cell receptors expanded by
149 the immunization regimens. We engineered a SARS-CoV-2 RBD variant that has two additional
150 glycans on the RBM which effectively block ACE-2 engagement (**Figure S6**). This variant
151 allowed us to bin SARS-CoV-2 spike-directed B cells into 3 populations: those that bound RBM
152 epitopes; those that bound the non-RBM epitopes on the RBD; and those that bound the
153 "remainder" of the spike protein (**Figure S7**). As a subset of SARS-CoV-2 spike-directed B cells,
154 the proportion of B cells specific for the SARS-CoV-2 RBM and non-RBM portion of the RBD
155 were considerably higher in the cohorts receiving the SARS-CoV-2 RBD homotrimer and RBD
156 homotrimer cocktail boosts ($p = 0.0070$) (**Figure 3A**). We also binned B cells that bound to both
157 the SARS-CoV-2 spike and either the SARS-CoV RBD or WIV1-CoV RBD (**Figure 3B**). We
158 found that cross-reactive IgG B cells predominantly targeted epitopes outside the RBM (the spike
159 remainder a result of the prime), mirroring what we observed in sera responses.
160
161 We next determined the neutralization potency from each of our cohorts using SARS-CoV-2,
162 SARS-CoV, and WIV1-CoV pseudoviruses (*8*). We observed a significant increase in WIV1-CoV
163 neutralization in the cohort that received the homotrimer cocktail boost compared to all other
164 cohorts ($p = 0.0012$) (**Figure 4A**). Importantly, this did not result in any significant loss in serum
165 neutralization potency against SARS-CoV-2 ($p = 0.6594$) (**Figure 4B**). We also observed higher
166 levels of SARS-CoV neutralization in the cohort that received the homotrimer cocktail boost as
167 compared to the cohort boosted with the SARS-CoV-2 RBD homotrimer and the SARS-CoV-2
168 monomeric RBD, though this trend was not significant ($p = 0.2370$) (**Figure 4C**). Thus, compared
169 to other cohorts, immunization with the RBD homotrimer cocktail resulted in a neutralizing
170 antibody response with both retrospective (e.g., SARS-CoV) and prospective breadth (e.g., WIV1-
171 CoV) even in context of preexisting immunity to SARS-CoV-2.
172
173 We wanted to determine what fraction of SARS-CoV-2 neutralization could be attributed to the
174 non-RBM RBD-directed response. To that end, we performed adsorption of pooled sera from each
175 cohort using MERS-CoV RBD (negative control), SARS-CoV-2 RBD, and a SARS-CoV-2 RBD
176 with four additional glycans engineered onto the RBM (SARS-CoV-2 ΔRBM RBD) (**Figure S6,**
177 **S8**). This construct was designed to block all RBM-directed antibodies as opposed to the one used
178 in flow cytometry, which only block antibodies that directly compete with ACE-2. Compared to

179 the samples adsorbed using MERS RBD, the samples adsorbed with either the SARS-CoV-2 RBD
180 or the SARS-CoV-2 ΔRBM RBD demonstrated a significant loss of SARS-CoV-2 neutralization
181 ($p = 0.0343$) (**Figure 4D, S9**). This indicates that non-RBM RBD-directed antibodies alone are
182 able to confer significant SARS-CoV-2 neutralization.
183
184 Here, we demonstrate that a cocktail of homotrimeric sarbecovirus RBDs can effectively generate
185 a neutralizing response to all components without a bias resulting from a SARS-CoV-2 imprinting
186 and without compromising SARS-CoV-2 neutralization. We find that this cross-neutralizing
187 antibody response is predominantly directed to RBD epitopes outside of the RBM. This is in
188 contrast to SARS-CoV-2 infection which does not appear to reliably generate cross-neutralizing
189 antibodies (*8*). Furthermore, previously reported vaccine candidates that aim to generate such a
190 cross-neutralizing response have not been shown to successfully refocus immunity towards cross-
191 neutralizing epitopes following an initial SARS-CoV-2 spike immunization (*26*). However, our
192 results suggest that following an initial SARS-CoV-2 exposure (e.g., commercial vaccination,
193 infection), subsequent boosting with a surveillance-informed selection of sarbecovirus RBD
194 homotrimers could result in pan-sarbecovirus immunity that protects against future pandemics.
195
196 **Acknowledgements**
197 We thank members of the Schmidt and Lingwood Laboratories for helpful discussions. We
198 acknowledge funding from NIH R01s AI146779 (AGS), AI124378, AI137057 and AI153098
199 (DL), and a Massachusetts Consortium on Pathogenesis Readiness (MassCPR) grant (AGS);
200 training grants: NIGMS T32 GM007753 (BMH and TMC); T32 AI007245 (JF); F31 Al138368
201 (MS). We thank Dr. Jason McLellan from University of Texas, Austin for the spike plasmid. We
202 thank Nir Hacohen and Michael Farzan for the kind gift of the ACE-2 expressing 293T cells to
203 ABB.
204
205 **Author Contributions**
206 Conceptualization, BMH, MS, JF, TMC, DL, AGS; Methodology, BMH, ECL, TMC, ABB, DL,
207 AGS; Investigation, BMH, MS, ECL, JF, ASY; Writing – Original Draft, BMH and AGS; Writing
208 – Review and Editing, all authors; Funding Acquisition, ABB, DL, AGS; Supervision, ABB, DL,
209 AGS.

210

211 **Materials and Methods**

212

213 **Receptor Binding Domain and Homotrimer Expression and Purification**

214 Receptor binding domains (RBDs) were designed based on the following sequences: SARS-CoV-
215 2 RBD (Genbank MN975262.1), SARS-CoV RBD (Genbank ABD72970.1), WIV1-CoV RBD
216 (Genbank AGZ48828.1), and MERS-CoV RBD (Genbank AHI48572.1). Constructs were codon
217 optimized by Integrated DNA Technologies, cloned into pVRC, and sequence confirmed by
218 Genewiz. The spike plasmid was obtained from Dr. Jason McLellan at the University of Texas,
219 Austin. It contained a Foldon trimerization domain as well as C-terminal HRV 3C-cleavable 6xHis
220 and 2xStrep II tags. Proteins were expressed in Expi293F cells (ThermoFisher) using
221 Expifectamine transfection reagents according to the manufacturer's protocols. All proteins
222 included a C-terminal HRV 3C-cleavable 8xHis tag to facilitate purification. Monomeric RBD
223 proteins also contained SBP tags, while homotrimeric constructs contained a previously published
224 hyperglycosylated GCN4 tag with two additional C-terminal cystines (*21*). Versions of the MERS-
225 CoV RBD, SARS-CoV-2 ΔRBM RBD with four additional putative glycosylation sites (Figure
226 S5), and SARS-CoV-2 RBD with C-terminal 8xHis and SNAP tags (*27*) were also generated.

227

228 Transfections were harvested after 5 days and clarified via centrifugation. Cell supernatants were
229 passaged over Cobalt-TALON resin (Takara) for immobilized metal affinity chromatography via
230 the 8xHis tag. After elution, proteins were passed over a Superdex 200 Increase 10/300 GL (GE
231 Healthcare) size exclusion column in PBS (Corning). Prior to immunization, 8xHis tags were
232 cleaved using HRV 3C protease (ThermoScientific). Cleaved protein was repurified using Cobalt-
233 TALON resin in order to remove the protease, cleaved tag, and any uncleaved protein.

234

235 **Fab and IgG Expression and Purification**

236 Genes for the variable domains of the heavy and light chains were codon optimized by Integrated
237 DNA Technologies and cloned into pVRC constructs containing the respective constant domains
238 as previously described (*28, 29*). Heavy-chain Fab constructs contained a HRV 3C-cleavable
239 8xHis tag, while heavy-chain IgG constructs contained HRV 3C-cleavable 8xHis and SBP tags.

240 Transfections and purifications were performed according to the same protocols used for the RBDs
241 and homotrimers.
242
243 **Biolayer Interferometry**
244 Biolayer interferometry (BLI) experiments were performed using a BLItz instrument (ForteBio).
245 Fabs were immobilized on a FAB2G biosensor (ForteBio), and CoV proteins were the analytes.
246 All proteins were diluted in PBS at room temperature. Titrations were performed to determine
247 binding affinities. Single-hit concentrations at 10 μM were performed to get an approximate K_D,
248 and then subsequent titrations at appropriate concentrations (at least three). A final K_D estimate
249 was determined using a global fit model with a 1:1 binding isotherm using vendor-supplied
250 software.
251
252 **Immunizations**
253 C57BL/6 mice (Jackson Laboratory) received 20 μg of protein adjuvanted with 50% w/v Sigma
254 adjuvant in 100 μL of inoculum. All immunizations were administered through the intraperitoneal
255 route. Mice were primed (day 0) and received boosting immunizations at day 21 and day 42.
256 following the initial prime (day 0). Serum samples were collected on day 56 for characterization,
257 with flow cytometry occurring between days 56 and 63. In this study, female mice aged 6-10 weeks
258 were used. All experiments were conducted with institutional IACUC approval (MGH protocol
259 2014N000252).
260
261 **Flow Cytometry**
262 Spleens were isolated from mice and single cell suspensions were generated by straining through
263 a 70 μm cell strainer. Red blood cells were removed by treating with ACK lysis buffer and washed
264 with PBS. Single cell suspensions were first stained with Aqua Live/Dead amine-reactive dye
265 (0.025 mg/mL) before applying the following B and T cell staining panel using the staining
266 approach described previously (*30, 31*). This included the following mouse-specific antibodies:
267 CD3-BV786 (BioLegend), CD19-BV421 (BioLegend), IgM-BV605 (BioLegend), IgG-
268 PerCP/Cy5.5 (BioLegend).
269

270 Streptavidin-conjugated fluorophores were used to label the SBP-tagged proteins as probes for
271 flow cytometry. For the cohorts that received the SARS-CoV-2 spike prime followed by either the
272 SARS-CoV-2 RBD homotrimer boost or the RBD homotrimer cocktail boost, the following probes
273 were generated: SARS-CoV-2 RBD-APC/Cy7 (streptavidin-APC/Cy7 from BioLegend), SARS-
274 CoV-2 spike-StreptTactin PE (StrepTactin PE from IBA Lifesciences), SARS-CoV-2 ΔRBM
275 RBD-PE/Cy5.5 (streptavidin-PE/Cy5.5 from BioLegend). The panel for the cohort that received
276 the SARS-CoV-2 spike prime followed by the RBD homotrimer cocktail boost also included
277 SARS-CoV RBD-APC (streptavidin-APC from BioLegend) and WIV1-CoV RBD-BV650
278 (streptavidin-BV650 from BioLegend). For the cohort that received three SARS-CoV-2 spike
279 immunizations, the following probes were generated: SARS-CoV-2 RBD-APC/Cy7 (streptavidin-
280 APC/Cy7 from BioLegend), SARS-CoV-2 spike-StreptTactin PE (StrepTactin PE from IBA
281 Lifesciences), SARS-CoV-2 ΔRBM RBD-APC (streptavidin-APC from BioLegend).
282 Conjugations were performed as previously described (*32*). Briefly, fluorescent streptavidin
283 conjugates were added in 5 increments with 20 minutes of incubation with rotation at 4°C in
284 between to achieve a final molar ratio of probe to streptavidin valency of 1:1. The final conjugated
285 probe concentration was 0.1 μg/mL. Flow cytometry was performed on a BD FACSAria Fusion
286 cytometer (BD Biosciences). Analysis of the resultant FCS files was conducted using FlowJo
287 (version 10).
288
289 **Serum ELISAs**
290 Serum ELISAs were performed by coating Corning 96-well clear flat bottom high bind microplates
291 with 100 μL of protein at 5 μg/mL in PBS. Plates were incubated overnight at 4°C. Coating
292 solution was removed, and plates were blocked using 1% BSA in PBS with 1% Tween for 60
293 minutes at room temperature. Blocking solution was removed. Sera were diluted 1:40 in PBS, and
294 5-fold serial dilution was performed. CR3022 IgG at a starting dilution of 5 μg/mL with 5-fold
295 serial dilution was used as a positive control. 40 μL of primary antibody solution was applied to
296 each well. Primary incubation occurred for 90 minutes at room temperature. Plates were then
297 washed three times with PBS-Tween. HRP-conjugated rabbit anti-mouse IgG antibody (Abcam)
298 at a concentration of 1:20,000 in PBS and a volume of 150 μL was used as a secondary antibody.
299 Secondary incubation occurred for 60 minutes at room temperature. Plates were then washed three

300 times with PBS-Tween. 1xABTS development solution (ThermoFisher) was applied as outlined
301 in the manufacturer's recommendations. Development was stopped after 30 minutes with a 1%
302 SDS solution. Plates were read at 405 nm using a SectraMax iD3 plate reader (Molecular Devices).
303
304 **Competition ELISAs**
305 Competition ELISAs were performed using a similar protocol to serum ELISAs. The primary
306 incubation consisted of 40 μL of the relevant IgG at 1 μM. Incubation occurred at room
307 temperature for 60 minutes. Mouse sera were then spiked in at a final concentration in the linear
308 range of the serum ELISA titration curve (1:800 for the cohort that received three SARS-CoV-2
309 RBD monomer immunizations, 1:12,800 for all other cohorts). Plates were incubated at room
310 temperature for an additional 60 minutes. The primary solution was removed, and plates were
311 washed three times using PBS-Tween. HRP-conjugated goat anti-mouse IgG, human/bovine/horse
312 SP ads antibody (Southern Biotech) was applied at a concentration of 1:4000 and a volume of 150
313 μL as a secondary antibody. Plates were then incubated, washed, and developed using the same
314 procedure as the serum ELISAs.
315
316 **ACE-2 Cell Binding Assay**
317 ACE-2 expressing 293T cells (*33*) (a kind gift from Nir Hacohen and Michael Farzan) were
318 harvested and washed with PBSF. Cells were allocated such that 200,000 cells were labelled for
319 each condition. Cells were incubated with 100 μL of 200 nM antigen in PBS for 60 minutes on
320 ice. Following two washes with PBS supplemented with 2% FBS, cells were incubated with 50
321 μL of 1:200 streptavidin-PE (Invitrogen) on ice for 30 minutes. Cells were washed twice and
322 resuspended in 100 μL of PBS supplemented with 2% FBS. Flow cytometry was performed using
323 a Stratedigm S1000Exi Flow Cytometer. FCS files were analyzed using FlowJo (version 10).
324
325 **Serum Adsorption**
326 SNAP-tagged (*27*) MERS-CoV RBD, SARS-CoV-2 ΔRBM RBD with four additional putative
327 glycosylation sites (Figure S5), and SARS-CoV-2 RBD were conjugated to SNAP-Capture Pull-
328 Down resin (New England BioLabs). For each conjugation, 20 μL of settled resin was resuspended
329 in 100 μL of protein at 1 mg/mL per the manufacturer's recommendations. Both MERS-CoV RBD

330 and SARS-CoV-2 RBD conjugation reactions also included 1 mM DTT to improve conjugation
331 efficiency. Wildtype-like reactivity to conformationally specific Fabs (CR3022, S309, and B38 for
332 SARS-CoV-2 RBD; m336 for MERS RBD) in the presence of 1 mM DTT was confirmed prior to
333 conjugation (*14, 16, 17, 34*). Conjugation occurred with rotation overnight at 4°C.
334
335 Following conjugation, the resin was washed 5 times with PBS via resuspension followed by
336 centrifugation and the removal of the supernatant. Sera from the mice in each cohort were pooled
337 and diluted 1:40 in PBS to a total volume of 100 μL. Diluted sera were added to the conjugated
338 resin and incubated with rotation overnight at 4°C. Resin was filtered from the sera following
339 incubation, and the adsorbed sera was used for neutralization assays and ELISAs.
340
341 **Serum Adsorption ELISAs**
342 Serum adsorption ELISAs were performed using a similar protocol to the serum ELISAs. For the
343 primary antibody incubation, adsorbed serum solution was diluted 1:2, and subsequent serial 5-
344 fold dilutions were generated. The remainder of the assay was performed according to the serum
345 ELISA procedure.
346
347 **Pseudovirus Neutralization Assay**
348 Serum neutralization against SARS-CoV-2, SARS-CoV, and WIV1-CoV was assessed using
349 lentiviral particles pseudotyped with the respective spike proteins as previously described (*8*).
350 Lentiviral particles were produced via transient transfection of 293T cells. The titers of viral
351 supernatants were determined via flow cytometry on 293T-ACE2 cells (*33*) and via the HIV-1
352 $p24^{CA}$ antigen capture assay (Leidos Biomedical Research, Inc.). Assays were performed in 384-
353 well plates (Grenier) using a Fluent Automated Workstation (Tecan). For mouse sera, samples
354 were initially diluted 1:9, with subsequent serial 3-fold dilutions. For sera that had previously been
355 adsorbed, the adsorbed sample was used for the first dilution, and serial 3-fold dilutions were
356 performed. Serum sample volume in each well was 20 μL, and 20 μL of pseudovirus containing
357 125 infectious units was added. The combination was incubated for 60 minutes at room
358 temperature. Afterwards, 10,000 293T-ACE2 cells (*33*) in 20 μL of media containing 15 μg/mL
359 polybrene was added. The plates were then incubated at 37°C for 60-72 hours.
360

361 A previously described assay buffer was used to lyse the cells (*35*). A Spectramax L luminometer
362 (Molecular Devices) was used to quantify luciferase expression. Percent neutralization at each
363 serum concentration was determined by subtracting background luminescence from cells only
364 sample wells, then dividing by luminescence of wells with only virus and cells. GraphPad Prism
365 was used to fit nonlinear regressions to the data, which allowed IC_{50} values to be calculated using
366 the interpolated 50% inhibitory concentration. IC_{50} values were calculated for all samples with a
367 neutralization value of at least 80% at the highest serum concentration.
368
369 **Statistical Analysis**
370 Statistical analyses and curve fitting were performed using GraphPad Prism (version 9). To
371 compare two populations of continuous variables without evidence of conforming to a normal
372 distribution, the non-parametric two-tailed Mann-Whitney U test was used. To compare multiple
373 populations meeting this description, the Kruskal-Wallis test was used with post hoc analysis using
374 Dunn's multiple comparison testing. The ratio paired t-test was used to compare two populations
375 with evidence of normality. P values were corrected for multiple comparisons, and a p value <
376 0.05 was considered significant.
377
378
379

References

1. F. Amanat, F. Krammer, SARS-CoV-2 Vaccines: Status Report. *Immunity* **52**, 583-589 (2020).
2. S. J. Anthony *et al*., Global patterns in coronavirus diversity. *Virus Evol* **3**, vex012 (2017).
3. M. F. Boni *et al*., Evolutionary origins of the SARS-CoV-2 sarbecovirus lineage responsible for the COVID-19 pandemic. *Nat Microbiol*, (2020).
4. National Research Council (US) Committee on Achieving Sustainable Global Capacity for Surveillance and Response to Emerging Diseases of Zoonotic Origin, *Sustaining Global Surveillance and Response to Emerging Zoonotic Diseases*. P. M. Keusch GT, Gonzalez MC, et al., Ed., (National Academies Press (US), Washington (DC), 2009), vol. 3.
5. S. Jiang, C. Hillyer, L. Du, Neutralizing Antibodies against SARS-CoV-2 and Other Human Coronaviruses. *Trends Immunol* **41**, 355-359 (2020).
6. L. Du *et al*., The spike protein of SARS-CoV--a target for vaccine and therapeutic development. *Nat Rev Microbiol* **7**, 226-236 (2009).
7. W. Yang *et al*., Estimating the infection-fatality risk of SARS-CoV-2 in New York City during the spring 2020 pandemic wave: a model-based analysis. *Lancet Infect Dis*, (2020).
8. W. F. Garcia-Beltran *et al*., COVID-19 neutralizing antibodies predict disease severity and survival. *medRxiv*, (2020).
9. D. M. Knipe, P. M. Howley, *Fields virology*. (Wolters Kluwer/Lippincott Williams & Wilkins Health, Philadelphia, PA, ed. 6th, 2013), pp. 2 volumes.
10. A. Z. Wec *et al*., Broad neutralization of SARS-related viruses by human monoclonal antibodies. *Science*, (2020).
11. M. Yuan *et al*., Structural basis of a shared antibody response to SARS-CoV-2. *Science*, (2020).
12. S. J. Zost *et al*., Potently neutralizing and protective human antibodies against SARS-CoV-2. *Nature*, (2020).
13. T. F. Rogers *et al*., Isolation of potent SARS-CoV-2 neutralizing antibodies and protection from disease in a small animal model. *Science*, (2020).
14. Y. Wu *et al*., A noncompeting pair of human neutralizing antibodies block COVID-19 virus binding to its receptor ACE2. *Science* **368**, 1274-1278 (2020).
15. L. Du *et al*., MERS-CoV spike protein: a key target for antivirals. *Expert Opin Ther Targets* **21**, 131-143 (2017).
16. M. Yuan *et al*., A highly conserved cryptic epitope in the receptor binding domains of SARS-CoV-2 and SARS-CoV. *Science* **368**, 630-633 (2020).
17. D. Pinto *et al*., Cross-neutralization of SARS-CoV-2 by a human monoclonal SARS-CoV antibody. *Nature* **583**, 290-295 (2020).
18. L. Dai *et al*., A Universal Design of Betacoronavirus Vaccines against COVID-19, MERS, and SARS. *Cell* **182**, 722-733 e711 (2020).
19. V. D. Menachery *et al*., SARS-like WIV1-CoV poised for human emergence. *Proc Natl Acad Sci U S A* **113**, 3048-3053 (2016).
20. J. M. Fonville *et al*., Antibody landscapes after influenza virus infection or vaccination. *Science* **346**, 996-1000 (2014).

21. K. Sliepen, T. van Montfort, M. Melchers, G. Isik, R. W. Sanders, Immunosilencing a highly immunogenic protein trimerization domain. *J Biol Chem* **290**, 7436-7442 (2015).
22. J. Pallesen *et al*., Immunogenicity and structures of a rationally designed prefusion MERS-CoV spike antigen. *Proc Natl Acad Sci U S A* **114**, E7348-E7357 (2017).
23. K. S. Corbett *et al*., SARS-CoV-2 mRNA vaccine design enabled by prototype pathogen preparedness. *Nature* **586**, 567-571 (2020).
24. J. Lan *et al*., Structure of the SARS-CoV-2 spike receptor-binding domain bound to the ACE2 receptor. *Nature* **581**, 215-220 (2020).
25. C. O. Barnes *et al*., SARS-CoV-2 neutralizing antibody structures inform therapeutic strategies. *Nature*, (2020).
26. A. A. Cohen *et al*., Mosaic RBD nanoparticle elicit neutralizing antibodies against SARS-CoV-2 and zoonotic coronaviruses. *bioXriv*, (2020).
27. A. Keppler *et al*., A general method for the covalent labeling of fusion proteins with small molecules in vivo. *Nat Biotechnol* **21**, 86-89 (2003).
28. A. G. Schmidt *et al*., Immunogenic Stimulus for Germline Precursors of Antibodies that Engage the Influenza Hemagglutinin Receptor-Binding Site. *Cell Rep* **13**, 2842-2850 (2015).
29. A. G. Schmidt *et al*., Viral receptor-binding site antibodies with diverse germline origins. *Cell* **161**, 1026-1034 (2015).
30. M. Sangesland *et al*., Germline-Encoded Affinity for Cognate Antigen Enables Vaccine Amplification of a Human Broadly Neutralizing Response against Influenza Virus. *Immunity* **51**, 735-749 e738 (2019).
31. G. C. Weaver *et al*., In vitro reconstitution of B cell receptor-antigen interactions to evaluate potential vaccine candidates. *Nat Protoc* **11**, 193-213 (2016).
32. N. Kaneko *et al*., Loss of Bcl-6-Expressing T Follicular Helper Cells and Germinal Centers in COVID-19. *Cell* **183**, 143-157 e113 (2020).
33. M. J. Moore *et al*., Retroviruses pseudotyped with the severe acute respiratory syndrome coronavirus spike protein efficiently infect cells expressing angiotensin-converting enzyme 2. *J Virol* **78**, 10628-10635 (2004).
34. T. Ying *et al*., Exceptionally potent neutralization of Middle East respiratory syndrome coronavirus by human monoclonal antibodies. *J Virol* **88**, 7796-7805 (2014).
35. E. Siebring-van Olst *et al*., Affordable luciferase reporter assay for cell-based high-throughput screening. *J Biomol Screen* **18**, 453-461 (2013).

460 **Figures**

461

462

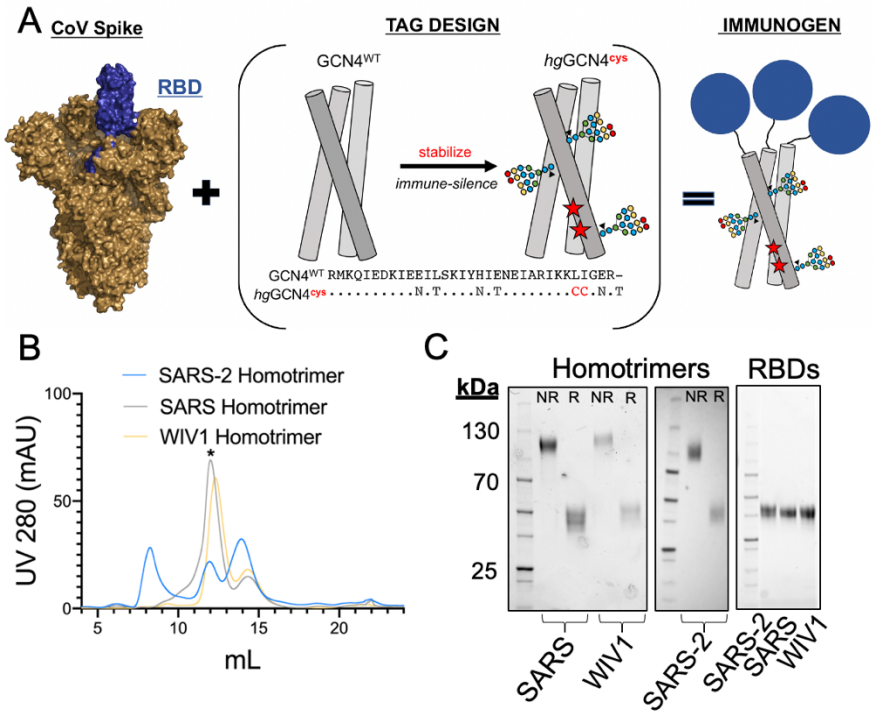

463

464

465 **Figure 1. Immunogen design, expression, and purification.** (**A**) Design schematic for
466 generating RBD homotrimers appended onto a cystine-stabilized (red stars) hyperglycosylated
467 GCN4 tag. (**B**) Representative size exclusion trace with (*) was the homotrimeric construct. (C)
468 SDS-PAGE analysis of purified homotrimers under non-reducing (NR) and reducing (R)
469 conditions. The engineered disulfide bond at the C-terminus of the hyperglycosylated GCN4 tag
470 separated under reducing conditions. Panel includes monomeric RBDs run under reducing
471 conditions for comparison.

472

A

Cohort ID	Day 0	Day 21	Day 42
Spike	SARS-2 Spike	SARS-2 Spike	SARS-2 Spike
RBD	SARS-2 RBD	SARS-2 RBD	SARS-2 RBD
Homotrimer	SARS-2 Spike	SARS-2 Homotrimer	SARS-2 Homotrimer
Cocktail	SARS-2 Spike	RBD Homotrimer Cocktail	RBD Homotrimer Cocktail

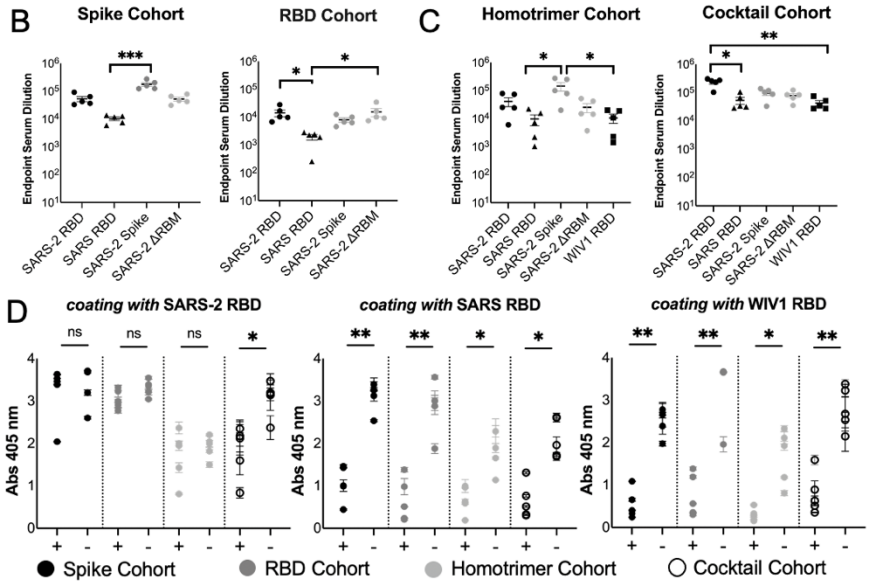

Figure 2. Serum response to immunization regimens. (**A**) Four immunization cohorts were used for this study (n=5 mice, per cohort). (**B, C**) Serum was assayed in ELISA at day 56 with different coronavirus antigens. (**D**) Competition ELISAs using S309 and CR3022 (+) or no IgG (-) and SARS-CoV-2, SARS-CoV, and WIV1-CoV RBDs as coating antigens. Sera from each cohort are color-coded. Statistical significance was determined using Kruskal-Wallis test with post-hoc analysis using Dunn's test corrected for multiple comparisons (* = $p < 0.05$, ** = $p < 0.01$, *** = $p < 0.001$); ns = not significant.

485

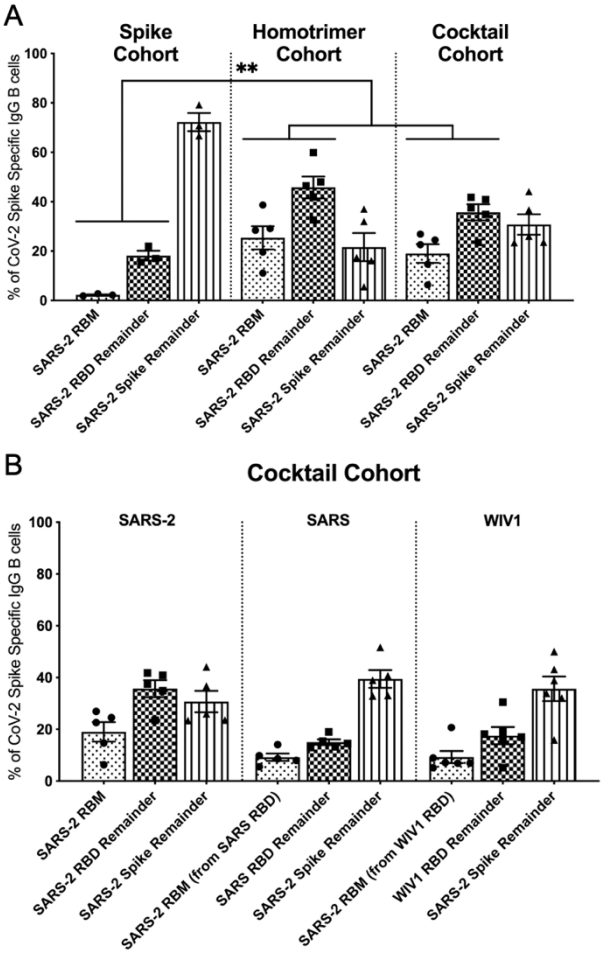

486

487

488 **Figure 3. SARS-CoV-2-specific IgG B cells expanded following immunization. (A)** Spike-
489 directed responses were binned into RBM, RBD remainder (excluding RBM epitopes), and spike
490 remainder (excluding RBD and RBM epitopes) populations using relevant probes in flow
491 cytometry. Data is shown as a percentage of total spike-specific IgG B-cells. We evaluated the
492 distribution of SARS-CoV-2 spike-directed responses and found evidence of focusing towards
493 non-spike RBD epitopes in the cohorts boosted with the SARS-CoV-2 RBD homotrimer and the
494 RBD homotrimer cocktail versus the cohort that received three SARS-CoV-2 spike immunizations
495 ($p = 0.0070$ via Mann-Whitney U test) (A). (**B**) The cocktail cohort was additionally assayed for
496 SARS-CoV or WIV1-CoV RBD reactivity, as described in (**A**).

497

498

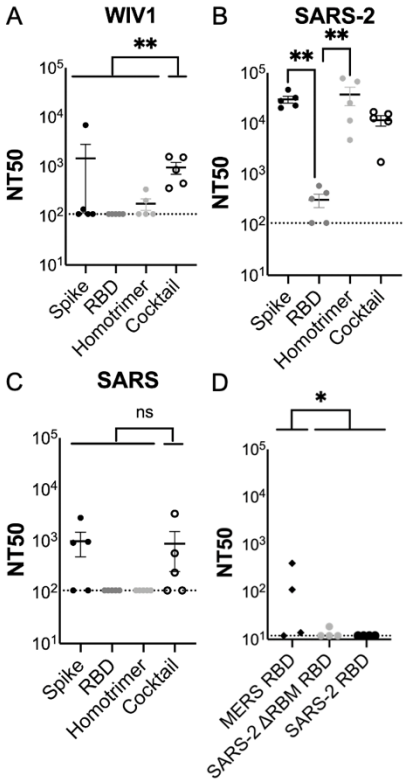

499

500

501 **Figure 4. Pan-sarbecovirus serum neutralization using pseudoviruses.** Day 56 serum from
502 each cohort was assayed for neutralization against (**A**) SARS-CoV-2, (**B**) SARS-CoV, and (**C**)
503 WIV1-CoV pseudoviruses. Statistical significance was determined using Kruskal-Wallis test with
504 post-hoc analysis using Dunn's test; * = $p < 0.05$, ** = $p < 0.01$. No significant difference in SARS-
505 CoV neutralization between the control cohorts and the RBD homotrimer cocktail boost cohort
506 (Mann-Whitney U test; $p = 0.2370$) (B), there was a significant difference in WIV1-CoV
507 neutralization (Mann-Whitney U test; $p = 0.0012$) (C). (**D**) Serum adsorption to remove antibodies
508 from pooled sera from each cohort directed towards MERS-CoV RBD (negative control), SARS-
509 CoV-2 ΔRBM RBD, and SARS-CoV-2 RBD. Sera adsorbed with MERS-CoV RBD had
510 significantly greater neutralization than those adsorbed with SARS-CoV-2 ΔRBM RBD and
511 SARS-CoV-2 RBD (Mann-Whitney U test; $p = 0.0343$). The spike cohort had the greatest MERS-
512 adsorbed neutralization.

513

514